Article ID：1004-4140（2008）04-0032-015

The Earthquake Volume from Body Waves

Seweryn J. Duda[1], Jaromír Janský[2]

1. Institut für Geophysik, Universität Hamburg, Bundesstrasse 55, 20146 Hamburg, Germany
2. Department of Geophysics, Charles University, Ke Karlovu 3, 12116 Prague, Czech Republic

Abstract: The propagation of seismic body waves is a linearly elastic process in most of the Earth body. Only in the region surrounding the earthquake focus nonlinear processes may be expected to take place as the result of the radiation and propagation of the waves. The investigation is concerned with the estimation of the dimension of the region in which nonlinear processes prevail.

Key words: body waves; strain; earthquake volume

CLC number: TP 315 **Document code:** A

The earthquake volume can generally be understood as the region inside the Earth affected most intensively by the process taking place around the focus. If for earthquakes the volumes were determined individually and independently, the earthquake volume would eventually prove to be a parameter of formidable tectonophysical significance, along with other parameters expressing the “size” or “strength” of the earthquake.

First estimates of the earthquake volume were based on the connotation that the hypocenters of aftershocks delineate the volume of the main shock of the earthquake sequence (Benioff, 1955). The earthquake volume so defined was determined for main shocks with magnitudes ranging for several orders. The approach led to volume estimates useful for a number of purposes (Bath and Duda, 1964). However, the interpretation of this earthquake volume in physical terms is not easy, even if the locations of the aftershocks were known completely and with highest accuracy.

In the present investigation the estimate of the earthquake volume is based on seismographic observations of body wave signals radiated from the earthquake focus. The practical implementation of this approach is facilitated by the availability of modern broadband seismographs. The amplitudes measured from the seismograms yield the ground motion at the point of observation in absolute units with higher accuracy than it was ever possible before.

For the purpose of the present investigation the earthquake volume is defined as the region inside the Earth in which the amplitudes of body waves (together with the dynamic strains generated by them) exceed a critical value. The critical value of the body wave amplitude (or the corresponding value of the dynamic strain) defines thus a closed surface containing the earthquake focus. The region inside this surface is called here the earthquake volume. A priori, any reasonable critical value can be assumed for the amplitude (or the dynamic strain). In practice, the critical value depends though on the knowledge of the physical properties of the medium controlling the propagation of the seismic signal along the ray path between the focus and the point of observation at the Earth surface. Also, the availability of a wave propagation theory enabling one to project the amplitude observed at the Earth surface along the ray path towards the focus is of paramount importance for the problem.

The present investigation is based solely on the linear theory of wave propagation. Thus, for

Recuved date: 2008-05-28。
Foundation item: Supported, in part, by Grant No: 205/07/0502 of the Grant Agency of the Czech Republic.

the critical amplitude (or dynamic strain) a value applies such that the wave propagation outside of the earthquake volume can be considered as a purely linear elastic process, while inside the volume nonlinearity prevails. No adequate observations are available which would permit to elucidate the process inside the so defined earthquake volume, and the application of non-linear theory of wave propagation would be of only limited value. In addition, exact information is lacking on when deformations of the Earth material can be considered as "small" to warrant the application of linear theory of elasticity. Consequently, only critical amplitudes assumed as reasonable (or corresponding critical dynamic strains) can define a surface separating the regions with linear and nonlinear behaviors in course of the radiation and propagation of seismic waves.

It is not difficult to imagine that the large amplitudes of the motion in the immediate vicinity of the focus will generate dynamic strains exceeding the strength of the material. Thereby two strengths have to be given consideration: such for longitudinal and such for transverse oscillations. Close to the source both dynamic strains act simultaneously, as parts of the near-field and far-field displacements. Only after the near-field displacements become negligible with respect to the far-field displacements, the dynamic dilatational strain and the dynamic shear strain act quasi-independently of each other and at different times.

Generally the strength of materials for dilatational strains is larger than the strength for shear strains. Consequently, for a fixed amplitude and period of the body waves, the earthquake volume estimated from longitudinal oscillations (*P*-waves) will differ from the volume estimated from transverse oscillations (*S*-waves). The ratio of the two volumes becomes thereby an additional parameter characterizing individual earthquakes.

In an earlier investigation Duda et al. (2000) presented isolines of *P*-wave amplitudes in the Earth mantle. The present investigation is the continuation in the sense that now the amplitude- and strain-regime at closer distances from the focus is given consideration. The two investigations are thus complementary with respect to each other.

Similarly as before, the amplitudes of body waves measured at the surface of the Earth are projected along the ray path in the direction of the earthquake focus, employing the zero order ray theory of wave propagation. From the amplitudes the dynamic strains are computed with emphasis on short distances from the focus. Distances are determined, at which – largely by assumption – the linear wave propagation starts. From this very distances the earthquake volume is estimated.

1 Method of computation

The dynamic strain produced by the oscillatory motion of seismic waves is time-variable, in accordance with the time-variability of the wave motion. Only the maximum value of the dynamic strain is deemed significant for the present purpose. In the case of a monochromatic wave the maximum dynamic strain is (Duda, 1970)

$$\varepsilon = \frac{4A}{\lambda} = \frac{4A}{vT} \tag{1}$$

Here A is the displacement amplitude of the wave, T – its period, λ – its wave length, and v – *P*- or *S*-wave velocity at the point M along the given ray path (Fig.1).

The *P*- or *S*-wave signal seen on seismograms is understood as the superposition of monochromatic waves, in accordance with Fourier's principle. In practice, the superposition principle applies outside the earthquake volume, as defined above, i.e. in the region where linear elasticity prevails during the wave propagation. In this region the displacement amplitudes, as well as the corresponding dynamic strains can be superposed, provided phase shifts are taken into account.

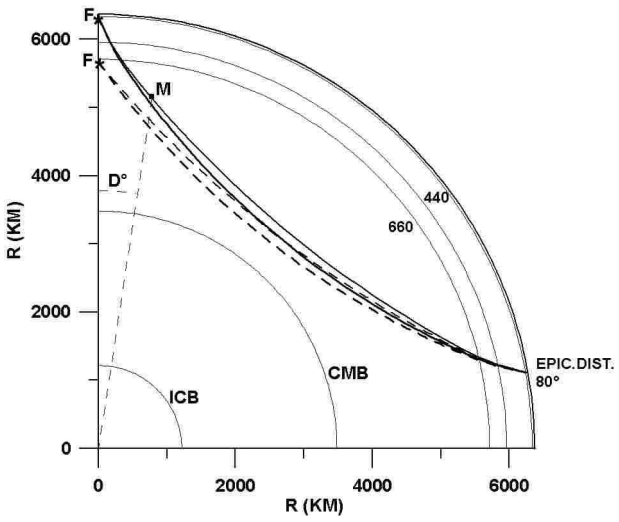

Fig.1 Structure of the Earth with ray paths of *P*-waves (heavy lines) and *S*-waves generated at the foci *F* (40 km and 700 km depth) and observed at 80° epicentral distance. *R* – distance from the centre of the Earth. Major discontinuities are shown in agreement with the IASP91-model (Kennett et al., 1995).

Referring to Fig.1, from the amplitude at the point *M* on the ray path the dynamic strain at this point is computed. In theory, the computation of either the amplitude or the dynamic strain is permitted at any point *M* on the ray path (with the exception of the focus *F*), if only the Earth material at the point obeys Hooke's law. Practically however, the computations become successively doubtful for points *M* approaching the source *F*. In the strict sence the linear theory of wave propagation is valid only at points *M* at which the amplitudes or dynamic strains remain below the critical value. Whatever critical value is assumed, its significance remains formalistic as long as no respective measurements can be performed. For this reason volume estimates are given for a range of critical values considered not to be unrealistic on the basis of laboratory experiments.

For the computation of the *P*-wave and *S*-wave amplitudes along the ray path we apply the two-point tracing zero-order ray method (Červený and Janský, 1983). The amplitude *A* at the point *M* is then:

$$A(M) = gVGqL^{-1}\exp\left(-\frac{\pi t^{*}}{T}\right) \tag{2}$$

Here, *g* characterizes the distribution of the displacement amplitudes on the unit sphere with its centre at the source *F*, whereby symmetric radiation from the source is assumed. *V* and *G* are given by the relations:

$$V = \left(\frac{v(S)\rho(S)}{v(M)\rho(M)}\right)^{\frac{1}{2}} \prod_{(k)} \left(\frac{v'(O_k)\,\rho'(O_k)}{v(O_k)\,\rho(O_k)}\right)^{\frac{1}{2}} \tag{3}$$

$$G = \prod_{(k)} \gamma_k \tag{4}$$

The products correspond successively to the individual transmission points O_1 - O_N at which

the ray intersects the boundaries on its way between the source F and the point M. In (3) $v(O_k)$ and $\rho(O_k)$ give the velocity and density at the point O_k on the side of the incident ray, and $v'(O_k)$ and $\rho'(O_k)$ - the same quantities on the other side of the boundary. Similarly $v(F)$ and $\rho(F)$ correspond to the source and $v(M)$ and $\rho(M)$ to the point M on the ray path. The symbol γ_k denotes the transmission coefficient at the point O_k. N is the total number of intersections of the ray path with the discontinuities. The quantity q depends on the position of the point M: if it is situated at the Earth's surface, q is the relevant conversion coefficient, and if it is situated inside a layer q is equal to one. Finally, the quantity L represents the geometrical spreading of the wave.

The period-dependent absorption of the body wave is assumed to have the form

$$\exp\left(-\frac{\pi t^*}{T}\right) \tag{5}$$

Here, t^* is given by the relation

$$t^* = \frac{1}{0.6\,366\tan^{-1}(1.5\,923\,T)} \int_S^M \frac{1}{vQ}\,\mathrm{d}s \tag{6}$$

where T is the period of the wave, Q is the quality factor as function of the distance of the point M from the Earth center, and the integral is calculated along the ray from the source F to the point M in Fig.1 (Duda and Yanovskaya, 1993; Yanovskaya and Duda, 1994; Lyskova et al., 1998).

Amplitudes of body waves at the Earth surface at an arbitrary teleseismic epicentral distance (no consideration is given in the paper to short epicentral distances, due to the generally complex nature of *P*- and *S*-wave signals in this distance range) can be converted to the respective amplitudes at a particular distance, applying the magnitude calibrating function for the given wave type (Duda and Yanovskaya, 1994). Thus, it suffices to make the computations of the amplitude variation along the ray path for a particular epicentral distance. This distance is taken in the following as equal to 80°, and the results of all amplitude computations are shown relative to the amplitude at this particular epicentral distance.

The results of the amplitude computation along the ray path are shown for two, in a way extreme, focal depths: 40 km and 700 km. Also, monochromatic radiation of the body waves is assumed, and the results are presented for body wave periods of 0.5 s, 4 s, and 32 s. The two extreme periods correspond to the periods observed for both *P*- and *S*-waves from earthquakes recorded on broadband seismograms (see Fig.9 below). Only direct body waves are taken into consideration, and eventual interference with waves reflected from discontinuities is disregarded. In view of other uncertainties, interpolations for other focal depths and wave periods are estimated to be permissible.

In the computations the spherically symmetrical velocity model for *P*- and *S*-waves IASP91 is used (Kennett and Engdahl, 1991), together with the spherically symmetrical anelasticity and density models AK135 (Kennett et al., 1995; Montagner and Kennett, 1996; Lyskova et al., 1998).

Under these conditions the relative amplitudes of the body waves along the ray paths are obtained.

2 Results of computations

Figs.2 and 3 refer to *P*- and *S*-waves respectively. The diagrams show the variation of the amplitudes of the waves along the ray paths as function of the angular distance between the source F and the point M (Fig.1). As reference amplitudes, the vertical component of the *P*-wave

and the horizontal part of radial component of the *S*-wave are used. No consideration is given to *SH*-waves. The amplitude variation along the respective paths is shown for the focal depths and wave periods as indicated. The epicentral distances vary from near the source up to 80°.

It is evident that the amplitudes of *P*-waves increase by 3-4 orders of magnitude from the point at 80° epicentral distance to near the focus (Fig.2). For the *S*-waves the respective increase amounts to factors ranging from 3 to 7 orders of magnitude, the most dramatic increase occurring for the *S*-wave with a period of 0.5 s. The increase of the amplitudes along the ray paths is due to the compensation for geometrical spreading and for the absorption of the waves, short-periodic *S*-waves showing the strongest effect.

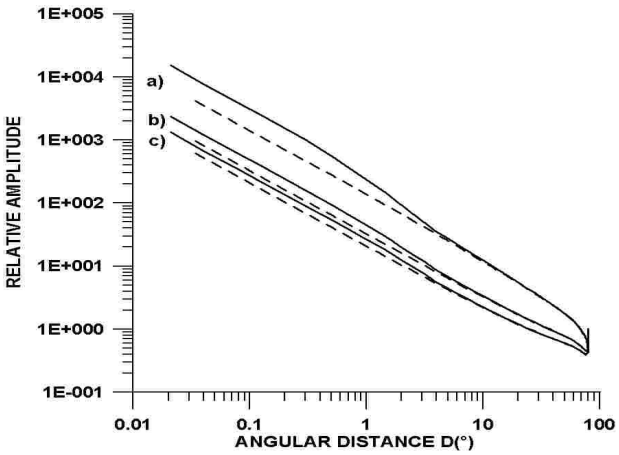

Fig.2 *P*-wave amplitudes along the ray path as function of angular distance *D* at the point *M* (Fig.1), in the distance range from 80° to near the source *F*. Source depth: 40 km—solid line, 700 km —dashed line. Wave periods: a) $T = 0.5$ s, b) $T = 4$ s, c) $T = 32$ s. As reference amplitude is taken the amplitude of the vertical component of the *P*-wave at 80° epicentral distance.

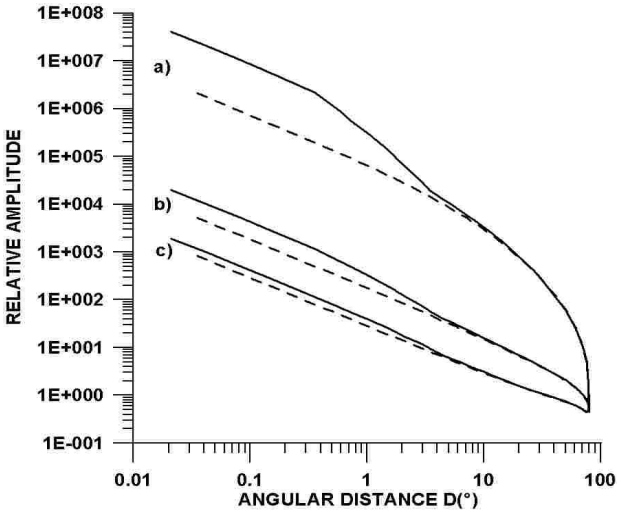

Fig.3 *S*-wave amplitudes along the ray path as function of angular distance *D* at the point *M* (Fig.1), in the distance range from 80° to near the source *F*. Source depth: 40 km—solid line, 700 km —dashed line. Wave periods: a) $T = 0.5$ s, b) $T = 4$ s, c) $T = 32$ s. As reference amplitude is taken the amplitude of horizontal part of the radial component of the *S*-wave at 80° epicentral distance.

Figs.4 and 5 show the amplitude variation as function of the linear distance along the ray, in the range from near the focus to 100 km. The reference amplitudes are the same as before. The large numerical values of the amplitudes suggest that nonlinear behavior of the material will start at some distance from the focus, and that the strength of the material will be exceeded, at even shorter distances. The aim of further computations is to estimate the distances from the focus within which non-linear behavior prevails. Only at distances larger than the critical one will the linear theory of wave propagation apply and the above computations of the amplitudes be valid.

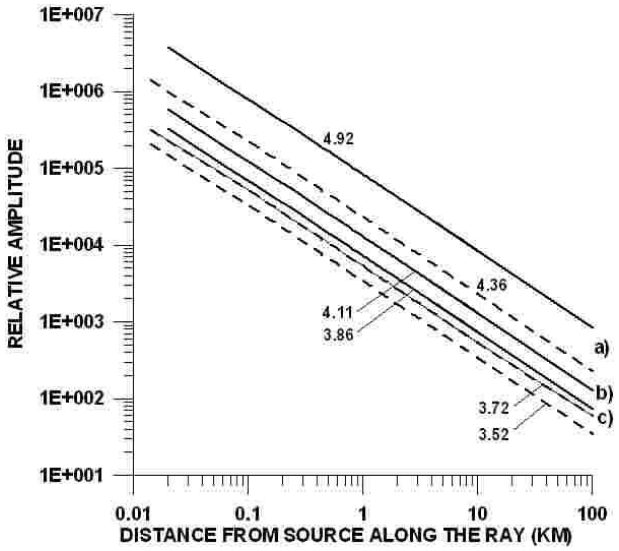

Fig.4 *P*-wave amplitudes as in Fig.2, as function of the linear distance of the point *M* from the source *F* along the ray path. The numerals give the coeficient *A* in the equation log(relative amplitude) = *A* + *B* log(distance), (*B* = 1; see text).

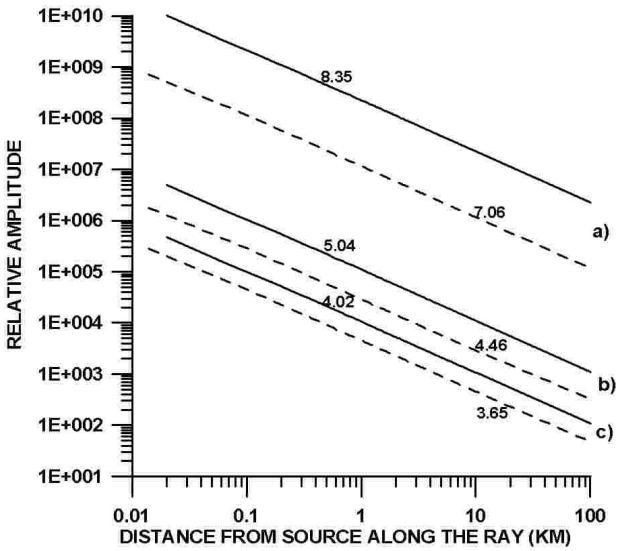

Fig.5 *S*-wave amplitudes as in Fig.3 as function of the linear distance of the point *M* from the source *F* along the ray path, in analogy to Fig.4.

It must be borne in mind that at short distances from the focus the near-field term of the displacement field becomes significant, and that *P*- and *S*-wave generated dynamic strains will not be separated in time (see above): the material of the Earth will be subjected here to dilatational and shear strains simultaneously.

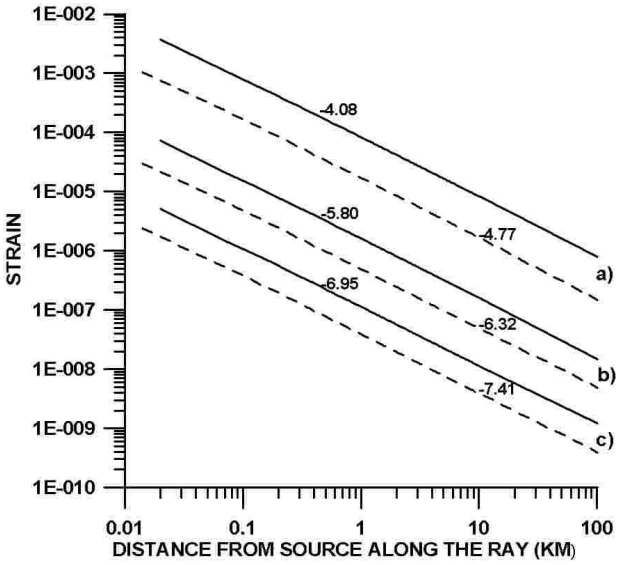

Fig.6 Dynamic longitudinal strains generated by *P*-waves from Fig.4. The reference *P*-wave amplitude (vertical component) is taken as 1 μm. Source depth: 40 km—solid line, 700 km—dashed line. Wave periods: a) $T = 0.5$ s, b) $T = 4$ s, c) $T = 32$ s. The numerals give the coeficient A in the equation log(strain) = $A + B$ log(distance), ($B = 1$).

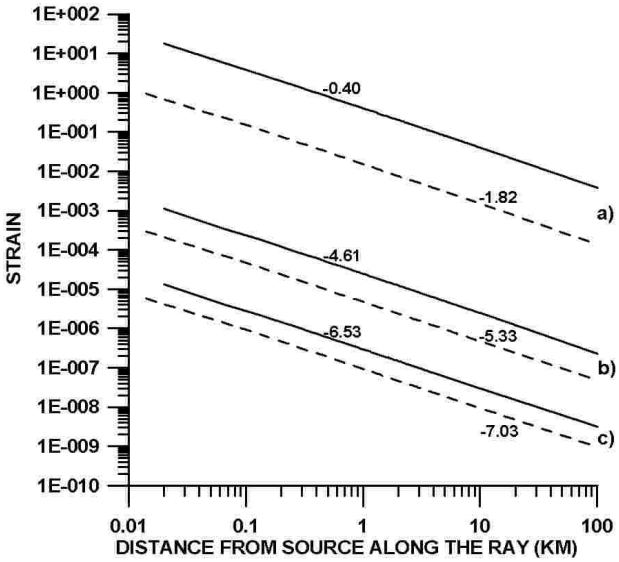

Fig.7 Dynamic shear strains generated by *S*-waves from Fig.5 in analogy to Fig.6. The reference *S*-wave amplitude (horizontal part of radial component) is taken as 1 μm.

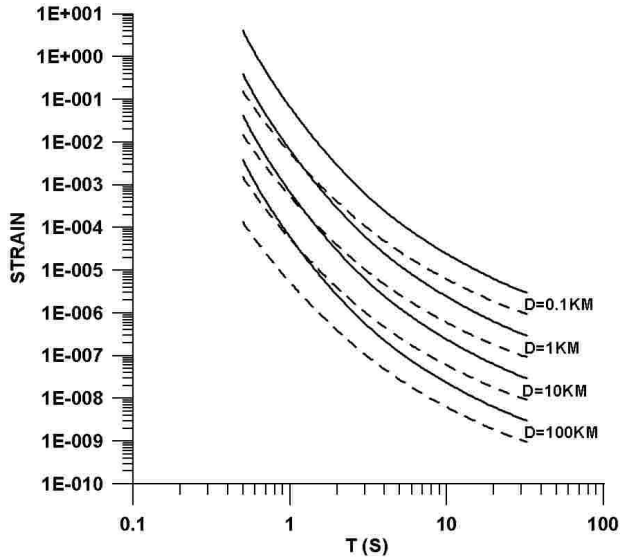

Fig.8 Shear strains as function of period, for source depths and distances along the ray path as indicated. Source depth: 40 km—solid line, 700 km—dashed line. The reference amplitude is taken as 1 μm. Compare with Fig.7.

For all practical purposes observations at teleseismic distances correspond to only the far-field term of the displacement field. Thus, the distance from the focus found in the present computations for a particular value of the dynamic strain will be *smaller* than the distance applying for the same strain value but for amplitudes resulting from the superposition of both the far-field *and* the near-field of the disturbance. The earthquake volume estimated from dynamic strains corresponding to the far-field only - as done here - (near-field observations as a rule not being available), will consequently be the *lower* limit for the factual value of the earthquake volume.

Fig.6 and 7 give the dynamic strains generated near the source by the *P*-waves and *S*-waves respectively. The strains are computed from (1) and from the amplitudes as given in Fig.4 and 5. Again, the numerical values of the strains at shortest distances from the source are significant only as long as Hooke's law underlying the computations is not violated.

In the figures the least square approximation of the curves are shown for the distance range as indicated. The dynamic strains (as also the wave amplitudes) are seen to decrease with the first power of the distance from the source ($b = 1$). Such a decrease is theoretically expected for the far-field amplitudes in a homogeneous medium. The agreement (within error limits) is due to the small variability of the structural constants of the medium surrounding the focus, together with the relatively high *Q*-values of the medium.

Finally, Fig.8 shows the dynamic shear strain as function of the period of the *S*-wave, with the distance from the focus as parameter. (The dynamic longitudinal strains show a less pronounced behavior). At a given distance from the focus it is seen that the dynamic shear strain is increasing by orders of magnitude with decreasing period. As mentioned earlier, it is assumed that the body waves have a displacement amplitude equal to 1 μm at the Earth surface at 80° epicentral distance. For the *S*-wave amplitudes actually observed at the Earth surface, the shear strains may be computed from the figure utilizing the Fig.5. (See next chapter.)

The critical dynamic strain separating regions with linearly elastic and non-linearly elastic behavior is not known, as the elasticity constants at the depths of the earthquake foci are not

accessible for measurements. Consequently, in the following discussion values for the critical strains can only be postulated.

3 Discussion of results of the strain computations

In Table 1 and 2 the relative amplitudes and the dynamic strains are shown for the focal depths of 40 km and 700 km, respectively, with the period of the wave and the distance along the ray path as parameters. E.g. for the focus at 40 km depth at a distance of 10 km, the amplitude of the *P*-wave with a period of 4 s inceases by a factor of 1300, and that of the *S*-wave - by a factor of 11000 with respect to that at the Earth surface at 80° epicentral distance. If the amplitude at the reference distance at the Earth surface is taken as 1 μm, the dynamic strains generated at the distance of 10 km from the focus amount to 1.6×10^{-7} and 2.4×10^{-6}, respectively. Such strains may be considered to be small enough for the linear wave propagation to prevail at the distance chosen, and at all larger distances.

Table 1 Amplitudes and dynamic strains of *P*- and *S*-waves as a function of period *T* and distance *D* from the source *F*. The source is located at the depth of 40 km. As reference, the vertical component of the *P*-wave and the horizontal (radial) component of the *S*-wave is used, respectively. The *P*- and *S*-wave velocities at this depth are 8.0 km/s and 4.5 km/s, respectively, λ gives the corresponding wave length.

	P-waves			*S*-waves		
Relative amplitudes for *F* at the depth of 40 km						
D(km)	$A(T=0.5\,\text{s})$ ($\lambda=4$ km)	$A(T=4\,\text{s})$ ($\lambda=32$ km)	$A(T=32\,\text{s})$ ($\lambda=256$ km)	$A(T=0.5\,\text{s})$ ($\lambda=2.3$ km)	$A(T=4\,\text{s})$ ($\lambda=18$ km)	$A(T=32\,\text{s})$ ($\lambda=144$ km)
	(Fig.4)			(Fig.5)		
0.1	8.3×10^{5}	1.3×10^{5}	7.2×10^{4}	2.2×10^{9}	1.1×10^{6}	1.0×10^{5}
1	8.3×10^{4}	1.3×10^{4}	7.2×10^{3}	2.2×10^{8}	1.1×10^{5}	1.0×10^{4}
10	8.3×10^{3}	1.3×10^{3}	7.2×10^{2}	2.2×10^{7}	1.1×10^{4}	1.0×10^{3}
100	8.3×10^{2}	1.3×10^{2}	7.2×10	2.2×10^{6}	1.1×10^{3}	1.0×10^{2}
Dynamic strains for reference amplitude of 1 μm						
D(km)	$\varepsilon(T=0.5\,\text{s})$	$\varepsilon(T=4\,\text{s})$	$\varepsilon(T=32\,\text{s})$	$\varepsilon(T=0.5\,\text{s})$	$\varepsilon(T=4\,\text{s})$	$\varepsilon(T=32\,\text{s})$
	(Fig.6)			(Fig.7)		
0.1	8.3×10^{-4}	1.6×10^{-5}	1.1×10^{-6}	4.0	2.4×10^{-4}	2.9×10^{-6}
1	8.3×10^{-5}	1.6×10^{-6}	1.1×10^{-7}	4.0×10^{-1}	2.4×10^{-5}	2.9×10^{-7}
10	8.3×10^{-6}	1.6×10^{-7}	1.1×10^{-8}	4.0×10^{-2}	2.4×10^{-6}	2.9×10^{-8}
100	8.3×10^{-7}	1.6×10^{-8}	1.1×10^{-9}	4.0×10^{-3}	2.4×10^{-7}	2.9×10^{-9}

For *P*-wave and *S*-wave displacement amplitudes at the Earth surface at 80° epicentral distance taken as equal to 1 μm, the *P*-wave magnitudes amount to 7,1, 6.2, and 5.3 at the periods of 0.5 s, 4 s, and 32 s, respectively. The magnitude figures are obtained thereby on the basis of the Gutenberg and Richter (1956) calibrating functions generally used in seismological practice. The functions are known though to apply in the strict sense only to *P*-waves with periods around 5 s (and *S*-waves with periods around 10 s; see below). We note here that the calibrating functions of Gutenberg and Richter (1956) are routinely applied by NEIS to *P*-wave observations in the period range 0.1 s ~ 3 s, which is lower by several octaves if compared to the period for which the Gutenberg and Richter calibrating function was originally designated. This fact must introduce inconsistencies in the routine estimates of body wave magnitudes.

For the focal depth of 700 km the corresponding magnitudes amount to 6.6, 5.7, and 4.8. The difference of the magnitudes at 0.5 s, and 32 s is seen to be 1.8 units for both focal depths.

On the other side, the application of period-dependend magnitude calibrating functions (Duda, Yanovskaya, 1994) yields for the amplitude of 1 μm at the Earth surface at 80° epicentral distance spectral magnitudes amounting to 7.85, 5.85, and 4.35 for the focal depth of 40 km, and spectral magnitudes amounting to 7.40, 5.70, and 4.55 for the focal depth of 700 km at the periods of 0.5 s, 4 s, and 32 s, respectively. The differences of the (spectral) magnitudes are here seen to be 3.50 and 2.80 units.

Table 2 Values as in Table 1, but for the source *F* situated at the depth of 700 km. *P*- and *S*-wave velocities at this depth are 10.9 km/s and 6.1 km/s, respectively.

	P-waves			*S*-waves		
Relative amplitudes for *F* at the depth of 700 km						
D(km)	$A(T=0.5\,s)$ ($\lambda=5.4$ km)	$A(T=4\,s)$ ($\lambda=44$ km)	$A(T=32\,s)$ ($\lambda=345$ km)	$A(T=0.5\,s)$ ($\lambda=3.0$ km)	$A(T=4\,s)$ ($\lambda=24$ km)	$A(T=32\,s)$ ($\lambda=195$ km)
	(Fig.4)			(Fig.5)		
0.1	2.3×10^{5}	5.3×10^{4}	3.4×10^{4}	1.1×10^{8}	2.9×10^{5}	4.5×10^{4}
1	2.3×10^{4}	5.3×10^{3}	3.4×10^{3}	1.1×10^{7}	2.9×10^{4}	4.5×10^{3}
10	2.3×10^{3}	5.3×10^{2}	3.4×10^{2}	1.1×10^{6}	2.9×10^{3}	4.5×10^{2}
100	2.3×10^{2}	5.3×10	3.4×10	1.1×10^{5}	2.9×10^{2}	4.5×10
Dynamic strains for reference amplitude of 1 μm						
D(km)	$\varepsilon(T=0.5\,s)$	$\varepsilon(T=4\,s)$	$\varepsilon(T=32\,s)$	$\varepsilon(T=0.5\,s)$	$\varepsilon(T=4\,s)$	$\varepsilon(T=32\,s)$
	(Fig.6)			(Fig.7)		
0.1	1.7×10^{-4}	4.9×10^{-6}	3.9×10^{-7}	1.5×10^{-1}	4.7×10^{-5}	9.3×10^{-7}
1	1.7×10^{-5}	4.9×10^{-7}	3.9×10^{-8}	1.5×10^{-2}	4.7×10^{-6}	9.3×10^{-8}
10	1.7×10^{-6}	4.9×10^{-8}	3.9×10^{-9}	1.5×10^{-3}	4.7×10^{-7}	9.3×10^{-9}
100	1.7×10^{-7}	4.9×10^{-9}	3.9×10^{-10}	1.5×10^{-4}	4.7×10^{-8}	9.3×10^{-10}

Needless to say, that real earthquakes do not produce at the Earth surface identical displacement amplitudes at periods ranging from 0.5 s ~ 32 s, a range of 6 octaves. Rather, the amplitude distributions as function of the wave period are a characteristic feature of the particular earthquake, requiring proper quantification (Nortmann and Duda, 1982, 1983).

To illustrate the point, two particular earthquakes are given consideration. The relevant source parameters of the earthquakes are shown in Table 3. Accordingly, the body-wave magnitudes m_b, as published by ISC, are identical for both earthquakes, i.e. on the basis of the m_b–values both earthquakes have identical strengths. The surface-wave magnitudes *MS* for the two eartquakes differ by 0.5 units, the smaller *MS*-value for the Kurile earthquake likely to be due to the greater focal depth of the earthquake.

Table 3 Parameters of earthquakes from two regions. The parameters are taken from sources as indicated.

KURILE		MEXICO	
6 Dec 1978; 14:02:01.0 Lat: 44.59 N; Long: 146.58 E; $h=91$ km	NEIS	29 Nov 1978; 19:52:47.6 Lat: 16.01 N; Long: 96.59 W; $h=18$ km	NEIS
$m_b=6.3$; $MS=7.1$	ISC	$m_b=6.3$; $MS=7.6$	ISC
$m_P^{max}(T)=6.8$, $m_S^{max}(T)=7.8$ at $T=3.5$ s from Fig.9		$m_P^{max}(T)=8.8$, $m_S^{max}(T)=9.0$ at $T=28$ s from Fig.9	

For a more consistent characterization of the strengths of the two earthquakes the broadband seismograms of the body-waves are utilized. The seismograms were obtained at the Central Seismological Observatory of the Federal Republic of Germany at Erlangen. Fig.9 displays the spectral magnitudes $m(T)$ for *P*- and for *S*-waves, as function of the wave period. For the determination of the spectral magnitudes $m(T)$ the broadband seismograms of the *P*- (vertical component) and the *S*-wave (horizontal component) were utilized. A sequence of one-octave filters with center periods ranging from 0.25 s ~ 128 s (10 octaves) was applied to the seismograms. From each of the 10 band pass seismograms the *P*-wave and *S*-wave amplitudes were found (if measureable), and the corresponding spectral magnitudes $m(T)$ determined. Thereby the period-dependent calibrating functions (Duda, Yanovskaya, 1994) were applied. The spectral magnitudes so obtained are displayed for the two earthquakes in the figure as function of the center period of the one-octave filters.

It is found that the maximum spectral magnitudes occur at largely different periods, namely at 3.5 s for the Kurile earthquake, and at 28 s for the Mexico earthquake. The periods corresponding to the respective maximum spectral magnitudes for *P*- and *S*-waves are seen to be identical. (This is not found to be the case in general, the maxima of *S*-waves for particular earthquakes occurring at either longer or shorter periods than these of *P*-waves).

The display of the spectral magnitudes in Fig.9 shows that the strengths of the two earthquakes are different, if the radiation at all relevant periods is taken into consideration. Also, m_b reflects only the radiation intensity around 1 s, being an unspecified average of the *P*-wave (*S*-wave are not taken into account in the seismological practice.) in the period range 0.1 s – 3 s (see above).

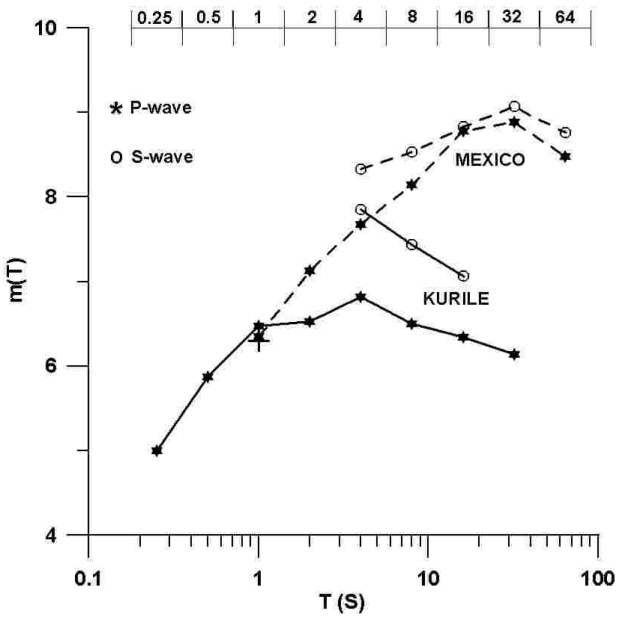

Fig.9 Spectral *P*-wave and *S*-wave magnitudes for two earthquakes as function of mid-band periods corresponding to one-octave band pass seismograms. The earthquake parameters are given in Table 3. The uppermost line shows the mid-band periods and the period ranges of the one-octave filters applied to the broadband records of the *P*-wave and *S*-wave. The cross at 1 s shows the m_b-value for the two earthquakes: according to ISC the m_b-values are identical for both earthquakes. See Table 3.

Evidently, the difference in the periods at which the maximum spectral magnitudes are found

indicates a dramatic difference of the focal processes during the two earthquakes. In particular, the earthquake volumes of the two earthquakes may be expected to differ significantly from each other.

The volumes are estimated from the *P*- and *S*-waves at periods revealing the strongest radiation intensity, i.e. from the amplitudes at the period of 3.5 s for the Kurile earthquake and of 28 s for the Mexico earthquake. In Table 4 the amplitudes at the Earth surface at 80° epicentral distance are shown for the respective maximum spectral magnitudes, the Mexico earthquake featuring clearly the larger amplitudes. Also, the distances are shown at which strains were attained, as indicated. Regardless of which strain value is taken as the critical one, the distance at which linear elasticity starts to prevail is larger for the Mexico earthquake, than for the Kurile earthquake. Qualitatively it may be said that the earthquake volume of the Mexico earthquake is larger than that of the Kurile earthquake, if the volume is determined for the period at which the maximum *P*-wave or *S*-wave radiation occurs.

Table 4 Spectral magnitudes $m(T)$ from Fig.9, the corresponding amplitudes A at the Earth surface (vertical component for the *P*-wave, radial component for the *S*-wave) and distances from the focus F along the ray, for the periods and dynamic strains as indicated.

Region	$m(T)$	A at 80°	D for strain 10^{-3}	D for strain 10^{-4}	D for strain 10^{-5}
KURILE	$m_P^{max}(3.5\,s)=6.8$	6 μ	0.01 km	0.1 km	1 km
	$m_S^{max}(3.5\,s)=7.8$	22 μ	0.54 km	5.4 km	54 km
	$m_P(28\,s)=6.1$	10 μ	0.001 km	0.01 km	0.1 km
	$m_S(28\,s)=6.7^*$	14 μ	0.004 km	0.04 km	0.4 km
MEXICO	$m_P^{max}(28\,s)=8.8$	2800 μ	0.31 km	3.1 km	31 km
	$m_S^{max}(28\,s)=9.0$	5600 μ	1.65 km	16.5 km	165 km
	$m_P(3.5\,s)=7.7$	26 μ	0.04 km	0.4 km	4 km
	$m_S(3.5\,s)=8.3$	148 μ	3.60 km	36.00 km	360 km

* from extrapolation; see Fig.9

Also, Table 4 shows that for the two earthquakes under consideration the distance at which a particular strain is attained is larger for *S*-waves than for *P*-waves. Consequently, the earthquake volume depends on the wave type utilized for its determination. And so, explosions and explosion-type earthquakes feature as a rule earthquake volumes larger if determined from *P*-waves. This is evident already from the fact that *P*-wave magnitudes for such events exceed the *S*-wave magnitudes. And vice versa, "slow" or "silent" earthquakes with barely measurable *P*-wave amplitudes, feature earthquake volumes larger if determined from *S*-waves.

The above conclusion is valid under the assumption that the amplitudes of the waves have been compensated for the geometrical effect due to the radiation patterns of both wave-types.

Based on Fig.9, Table 4 shows also the spectral magnitudes of the Kurile earthquake at the period corresponding to the maximum magnitudes of the Mexico earthquake (28 s), as well as the spectral magnitudes of the Mexico earthquake at the period corresponding to the maximum magnitudes of the Kurile earthquake (3.5 s). As before, the distances D are found for both wave types to be larger for the Mexico earthquake.

As mentioned before, Figs.6 and 7 apply for a reference amplitude of 1 μm at the surface at 80° epicentral distance. If for a particular earthquake the amplitude at the reference distance will be different by a factor of k, the distance found in Figs.6 and 7 for a given strain value has to be multiplied by the factor k, in order to obtain the distance corresponding to the earthquake. E.g. if the observed amplitude is larger (or smaller) by one order of magnitude at the given period of the

wave, the respective strain value will be attained at a distance 10 times larger (or smaller) than is the distance from Figs.6 and 7. Also, if the strain in Figs.6 and 7 at a given distance has a certain value, it will be k times larger (or smaller) at this distance, if the observed amplitude at the reference distance of 80° epicentral distance is k times larger (or smaller). In this way the distances from the source for a given strain, or strains at a given distance from the source may be found from Figs.6 and 7 for an arbitrary value of the amplitude at the respective period and at 80° epicentral distance.

Table 5 Earthquake volume V (in m^3) estimated from the distances at which the given dynamic strains were produced. The dynamic strains resultated from the *P*- and *S*-waves at periods corresponding to the maximum amplitudes (3.5 s for the Kurile earthquake and 28 s for the Mexico earthquake).

Region	m	V for strain 10^{-3}	V for strain 10^{-4}	V for strain 10^{-5}
KURILE	$m_P^{max}(3.5\,s)=6.8$	4.2×10^{3}	4.2×10^{6}	4.2×10^{9}
	$m_S^{max}(3.5\,s)=7.8$	6.6×10^{8}	6.6×10^{11}	6.6×10^{14}
MEXICO	$m_P^{max}(28\,s)=8.8$	1.3×10^{8}	1.3×10^{11}	1.3×10^{14}
	$m_S^{max}(28\,s)=9.0$	1.9×10^{10}	1.9×10^{13}	1.9×10^{16}

4 Conclusions

The distances at which *P*-waves and *S*-waves produce a given dynamic strain generally differ from each other. Consequently, the earthquake volume of a given earthquake has different values for the two kind of body waves. Also, assuming identical (for all periods) displacement amplitudes at the Earth surface at the reference distance, the above distances show a clear dependence on the period of the given body wave, the distances and the volumes being as a rule larger for shorter waves.

E.g. from Fig.6 it is seen that the 4 s *P*-wave having an amplitude of 1 μm at 80° produces a strain of 10^{-4} at a distance of about 20 m from the focus. The corresponding 0.5 s wave however generates the same strain at a distance of about 1 km, and the 32 s wave - at a distance of less than 1 m. If the critical distance is taken as the radius of a sphere, the volume of the sphere will be largest for the 0.5 s wave, and negligible for the 32 s wave. In other words, the 32 s wave propagation will be a linearly elastic process at practically all distances along the ray path, while the 0.5 s wave propagation will be a non-linear process at small, and linear process at larger distances.

From Fig.7 in turn it is seen that for the 4 s *S*-wave the strain of 10^{-4} is attained at a distance of 150 m, and for the 0.5 s *S*-wave – at a distance larger than 100 m. The distance for the 32 s *S*-wave is negligibly small again. It is concluded that non-linear behavior of the Earth material results primarily from the action of shortperiodic waves, notably *S*-waves.

In particular it is found for the Kurile earthquake (Table 4) that the strain of e.g. 10^{-4} was produced at the distances of 0.1 km and 5.4 km by the *P*- and *S*-waves respectively, both having the period of 3.5 s. The corresponding distances for the Mexico earthquake are 3.1 km and 16.5 km, but for the period of 28 s. The computation confirms that the earthquake volume of the Mexico earthquake was larger than that of the Kurile earthquake. Also, the computations quantify the difference of the volume.

In addition, the computations quantify the destructiveness of the body waves in the period range observed at teleseismic distances. Here, the destructiveness is understood as the potential of the wave to induce non-linear behavior of the Earth material. For constant displacement amplitudes at the Earth surface, the destructiveness of *S*-waves is as a rule higher than that of

P-waves, and for *S*-waves the destructiveness is as a rule highest for short periods.

It is known though that shortperiodic *S*-waves are often not observed at teleseismic distances, a fact attributed to the higher absorption in the region of the Earth where linear wave propagation prevails.

In the region of non-linear wave propagation the energy carried by shortperiodic *S*-waves is additionally used to shatter the material in the region surrounding the focus. On this basis the process of faulting during "normal" earthquakes may be understood as a progression of non-linear behavior of the material primarily caused by shortperiodic *S*-waves. Accordingly, the starting point of faulting radiates waves which cause dynamic shear strains at neighboring points. At predisposed point, usually located on the fault plane, the strains cause the strength of the material to be exceeded and the points will in turn radiate waves causing dynamic shear strains in the surrounding medium. In this way the fault plane is activated, embedded in a region in which further non-elastic processes prevail during the wave radiation and propagation. The region merges eventually into the one in which the wave propagation takes place in accordance with the linear theory. The above picture is in agreement with observations of the faulting velocity, which generally does not exceed the velocity of *S*-waves.

In case of seismic events not producing *S*-waves with sufficient intensity, as e.g. explosions, the non-linear behavior of the material around the focus is produced primarily by shortperiodic *P*-waves. Due to the higher strength of the material for longitudinal strains however the dimensions of the non-linear region around the focus will prove in this case to be smaller for a given amplitude at the Earth surface.

Disregarding the geometrical effects of the radiation pattern, the intensity of *P*-waves and of *S*-waves radiation at a particular period do vary in a measurable way from earthquake to earthquake. To measure the differences requires the independent determination of *P*-wave and *S*-wave magnitudes. In other words, *P*-wave magnitudes may be expected to correlate with *S*-wave magnitudes at a given period only in very broad terms. Modern observations of body wave radiation make it possible to quantify the respective radiation characteristics of earthquakes. Thereby, the maximum *P*-wave and the maximum *S*-wave magnitudes reflect the size of the non-elastic region surrounding the earthquake focus.

Acknowledgements: The investigation was performed under the partnership agreement between the University of Hamburg and the Charles University in Prague. This work was supported, in part, by Grant No: 205/07/0502 of the Grant Agency of the Czech Republic.

References

Benioff H. 1955. Mechanism and strain characteristic of the White Wolf fault as indicated by the aftershocks sequence[J]. Calif Dept Nat Resources, Division of Mines, Bull. 171, Pt. II: 199-202.

Bath M, Duda S J. 1964. Earthquake volume, fault plane area, seismic energy, strain, deformation and related quantities[J]. Ann Geofis, 17: 353-368.

Červený V, Janský J. 1983. Ray amplitudes of seismic body waves in inhomogeneous radially symmetric media[J]. Studia geoph et geod, 27: 9-18.

Duda S J. 1970. The earthquake volume[J]. Bull Seism Soc Am, 60: 1479-1489.

Duda S J, Yanovskaya T B. 1993. Spectral amplitude-distance curves for *P*-waves: effects of velocity and *Q*-distribution[J]. Tectonophysics, 217: 255-265.

Duda S J, Yanovskaya T B. 1994. Calibrating functions for *P*-wave spectral magnitudes[J]. Acta Geoph Polonica, 42: 293-306.

Duda S J, Janský J, Kvasnicka M. 2000. *P*-wave amplitudes and dynamic strains inside the Earth[J]. Acta Geoph. Polonica, 48: 179-193.

Gutenberg B, Richter C F. 1956. Magnitude and energy of earthquakes[J]. Ann Geofis, 9: 1-15.
ISC – International Seismological Centre, Thatcham, Berkshire, U.K.
Kennett B L N, Engdahl E R. 1991. Traveltimes for global earthquake location and phase identification[J]. Geophys J Int, 105: 429-465.
Kennett B L N, Engdahl E R, Buland R. 1995. Constraints on seismic velocities in the Earth from traveltimes[J]. Geophys J Int, 122: 108-124.
NEIS – National Earthquake Information Service of the US Geological Survey[C]. Boulder, Colorado, USA.
Lyskova E L, Roslov Y V, Yanovskaya T B, et al. 1998. Verification and refinement of spectral magnitude calibrating functions for *P*-waves[J]. J Seismol, 2: 117-124.
Montagner J P, Kennett B L N. 1996. How to reconcile body-wave and normal-mode reference earth models[J]. Geophys J Int, 125: 229-248.
Nortmann R, Duda S J. 1982. The amplitude spectra of *P*- and *S*-waves and the body wave magnitude of earthquakes[J]. Tectonophysics, 84: 17-32.
Nortmann R, Duda S J. 1983. Determination of spectral properties of earthquakes from their magnitudes[J]. Tectonophysics, 93: 251-275.
Yanovskaya T B, Duda S J. 1994. *Q*(*T*) for short periods from broadband observations of *P*-waves[J]. Acta Geophys Pol, 42: 281-292.

地震体积的体波研究

Seweryn J. Duda[1], Jaromír Janský[2]

1. Institut für Geophysik, Universität Hamburg, Bundesstrasse 55, 20146 Hamburg, Germany
2. Department of Geophysics, Charles University, Ke Karlovu 3, 12116 Prague 2, Czech Republic

摘要：在地球内部的大部分区域地震体波的传播是线弹性过程，仅在震源周围区域由于波的辐射和传播效应可能导致非线性。本研究主要涉及对非线性过程占优势区域的尺度估计。

关键词：体波；应变；体积

Biography: Seweryn J. Duda (1933－), Male, Professor Emeritus, Hamburg University, Hamburg, Germany. Research interest: Earthquake Seismology, in particular Quantification of Earthquakes, Tel: +4950662780, E-mail: seweryn.duda@zmaw.de.
Jaromír Janský (the corresponding author, 1936－), Male, Dr. Researcher－part time, Charles University, Prague, Czech Republic. Research interest: Body Waves propagation, Earthquake location, Tel: +42021911444, E-mail: jansky@seis.karlov.mff.cuni.cz.